The Astrophysical Journal, 836:116 (8pp), 2017 February 10 https://doi.org/10.3847/1538-4357/836/1/116


# X-Ray Spectral Properties of Seven Heavily Obscured Seyfert 2 Galaxies

S. Marchesi[1], M. Ajello[1], A. Comastri[2], G. Cusumano[3], V. La Parola[3], and A. Segreto[3]
[1] Department of Physics & Astronomy, Clemson University, Clemson, SC 29634, USA; smarche@clemson.edu
[2] INAF—Osservatorio Astronomico di Bologna, via Ranzani 1, I-40127 Bologna, Italy
[3] INAF—Istituto di Astrofisica Spaziale e Fisica Cosmica, Via U. La Malfa 153, I-90146 Palermo, Italy
*Received 2016 September 19; revised 2017 January 11; accepted 2017 January 14; published 2017 February 13*

## Abstract

We present the combined *Chandra* and *Swift*-BAT spectral analysis of seven Seyfert 2 galaxies selected from the *Swift*-BAT 100 month catalog. We selected nearby ($z \leqslant 0.03$) sources lacking a *ROSAT* counterpart that never previously been observed with *Chandra* in the 0.3–10 keV energy range, and targeted these objects with 10 ks *Chandra* ACIS-S observations. The X-ray spectral fitting over the 0.3–150 keV energy range allows us to determine that all the objects are significantly obscured, with $N_{\rm H} \geqslant 10^{23}\,{\rm cm}^{-2}$ at a >99% confidence level. Moreover, one to three sources are candidate Compton-thick Active Galactic Nuclei (CT-AGNs; i.e., $N_{\rm H} \geqslant 10^{24}\,{\rm cm}^{-2}$). We also test the recent spectral curvature method developed by Koss et al. to find candidate CT-AGNs, finding a good agreement between our results and their predictions. Because the selection criteria we adopted were effective in detecting highly obscured AGNs, further observations of these and other Seyfert 2 galaxies selected from the *Swift*-BAT 100 month catalog will allow us to create a statistically significant sample of highly obscured AGNs, therefore providing a better understanding of the physics of the obscuration processes.

*Key words:* galaxies: active – galaxies: nuclei – X-rays: galaxies

## 1. Introduction

The Cosmic X-ray Background (CXB; i.e., the diffused X-ray emission observed in the energy range going from 1 to ∼200–300 keV), is mainly caused by unobscured and obscured Active Galactic Nuclei (AGNs; e.g., Alexander et al. 2003; Gilli et al. 2007; Treister et al. 2009). However, while the unobscured AGN population responsible for the CXB emission at <10 keV has been almost completely detected, only ∼30% of the CXB at its peak (∼30 keV, Ajello et al. 2008) has been directly detected thanks to several surveys with the *NuSTAR* telescope (Aird et al. 2015; Civano et al. 2015; Harrison et al. 2015; Mullaney et al. 2015). Moreover, while theoretically Compton-thick (CT-) AGNs (i.e., sources with absorbing column density $N_{\rm H} \geqslant 10^{24}\,{\rm cm}^{-2}$) are expected to be numerous (see, e.g., Risaliti et al. 1999) and responsible for ∼10%–25% of the CXB emission at its peak; thus, the fraction of CT-AGNs detected with respect to the total number of AGNs is so far ∼5% (Comastri 2004, p. 245; Della Ceca et al. 2008).

For AGNs with column densities $\leqslant 10^{25}\,{\rm cm}^{-2}$, a fraction of direct nuclear emission can be observed at ⩾10 keV; for larger column densities, the only observable component in the same energy range is the scattered, indirect one (see, e.g., Matt et al. 1999; Yaqoob et al. 2010). Consequently, a complete census of the CT-AGN population requires deep observations above 10 keV. Burlon et al. (2011) analyzed the 15–55 keV spectral properties of a complete sample of AGNs at $z < 0.1$ detected by *Swift*-BAT, and found that the observed fraction of CT-AGNs in this sample was ∼5%. However, in the same work it was noted that even above 10 keV, the AGN emission is strongly suppressed by absorption and Compton scattering. Therefore, the ∼5% fraction of obscured AGNs observed in most works in the literature could not be intrinsic, but could instead be related to an observational bias. In fact, the modeling of this selection effect in Burlon et al. (2011) suggests that the intrinsic CT-AGN population accounts for about 20% of the whole AGN population. A similar intrinsic fraction of CT sources was also computed by Brightman & Nandra (2011) and Vasudevan et al. (2013).

While detecting CT-AGNs remains a challenging task, in the last 10 years several works were able to detect at least part of these extremely obscured objects. Because the energy range is observable in the 0.5–10 keV band at $z > 1$ the >10 keV, deep-field surveys with *Chandra* and XMM-*Newton* can detect CT-AGNs at $z > 1$ (see, e.g., Georgantopoulos et al. 2013; Vignali et al. 2014; Buchner et al. 2015; Lanzuisi et al. 2015). A further step in detecting and analyzing candidate CT-AGNs was the launch of *NuSTAR*, which allowed single sources to be studied with unprecedented statistics in the 5–50 keV band (see, e.g., Arévalo et al. 2014; Baloković et al. 2014; Gandhi et al. 2014; Annuar et al. 2015; Bauer et al. 2015; Koss et al. 2015; Lansbury et al. 2015; Boorman et al. 2016; Puccetti et al. 2016; Ricci et al. 2016).

AGN obscuration is usually linked to the presence of a so-called dusty torus (i.e., the gas and dust material surrounding the AGN accretion disk and responsible for the obscuration). This material is not continuously distributed, but more likely a clumpy distribution of optically thick dusty clouds (e.g., Elitzur & Shlosman 2006; Risaliti et al. 2007; Hönig & Beckert 2007; Nenkova et al. 2008). In the disk outflow scenario (Emmering et al. 1992) the obscuration is caused by a clumpy disk wind and can be described using two main parameters: the AGN luminosity and Eddington ratio. This model predicts that in the low-luminosity regime (i.e., at bolometric luminosities $L_{\rm bol} \leqslant 10^{42}\,{\rm erg\,s}^{-1}$) the cloud outflow process cannot be sustained by the AGNs and the broad-line region (BLR), so the dusty clouds should both disappear (Nicastro 2000; Elitzur & Ho 2009). This prediction was observationally confirmed by Burlon et al. (2011), who found a decrease in the fraction of obscured AGNs detected by *Swift*-BAT at $L_{15-55\,{\rm keV}} \leqslant 10^{43}\,{\rm erg\,s}^{-1}$. A similar behavior may be linked to a change in the AGN accretion regime, switching from an optically thick, geometrically thin disk (e.g., Shakura & Sunyaev 1973) to a radiatively inefficient accretion flow

**Table 1**
Summary of the Sources in Our Sample

| *Swift*-BAT ID | Source name | R.A. (deg (J2000)) | Decl. (deg (J2000)) | $z$ | $L_{15-55\ \mathrm{keV}}$ (erg s$^{-1}$) | Obs ID | Obs Date |
|---|---|---|---|---|---|---|---|
| J1253.5–4844 | NGC 4785 | 193.3639 | −48.7492 | 0.0123 | $2.3 \times 10^{42}$ | 18074 | 2016 Apr 16 |
| J1024.6–2332 | ESO 500-G034 | 156.1310 | −23.5530 | 0.0122 | $1.8 \times 10^{42}$ | 18075 | 2016 Feb 08 |
| J0333.7–0504 | NGC 1358 | 53.4153 | −5.0894 | 0.0134 | $2.0 \times 10^{42}$ | 18076 | 2015 Nov 21 |
| J0324.8–6043 | ESO 116-G018 | 51.2210 | −60.7384 | 0.0185 | $2.5 \times 10^{42}$ | 18077 | 2016 Aug 05 |
| J0448.9–5739 | ESO 119-G008 | 72.2364 | −57.6592 | 0.0229 | $4.4 \times 10^{42}$ | 18078 | 2016 Jul 09 |
| J2234.9–2543 | ESO 533-G050 | 338.7076 | −25.6769 | 0.0264 | $1.1 \times 10^{43}$ | 18079 | 2016 May 22 |
| J1539.0+1701 | NGC 5972 | 234.7257 | 17.0262 | 0.0297 | $1.0 \times 10^{43}$ | 18080 | 2016 Apr 04 |

**Note.** The *Swift*-BAT IDs all come from the Palermo BAT Catalog Fourth Version (4PBC). "Obs ID" and "obs date" refer to the *Chandra* Observations.

(e.g., Narayan & Yi 1994; Blandford & Begelman 1999). However, a recent work by Brightman et al. (2015) found no evidence of a decrease of the obscured AGN fraction at low luminosities. Consequently, the detection and study of low-luminosity, highly obscured AGNs becomes strategic to better understand the physics of the torus and the accretion disk.

In this work, we analyze the 0.3–150 keV spectra of seven nearby Seyfert 2 galaxies detected with *Swift*-BAT in the 15–150 keV band and reported in the *Swift*-BAT 100 month catalog. These sources have $L_{15-55\ \mathrm{keV}} \leqslant 10^{43}$ erg s$^{-1}$. We obtained a 10 ks follow-up with *Chandra* ACIS-S in the 0.3–7 keV band for each object in the sample. The combination of *Chandra* and *Swift*-BAT observations provides an ideal data set to properly characterize the main physical features of these sources, which are all expected to be heavily obscured and even CT. In Section 2 we describe our sample and the data reduction procedure adopted for the *Chandra* data. In Section 3 we present the result of the spectral fitting procedure, a physical analysis of the best-fit models and a comparison with previous results for two of the seven sources. Finally, in Section 4 we discuss our results, focusing on the effectiveness of our selection procedure in detecting highly obscured AGNs.

Throughout this work, we adopt a cosmology with $\Omega_m = 0.27$, $\Omega_\Lambda = 0.73$, and $H_0 = 71$ km s$^{-1}$ Mpc$^{-1}$. Errors are quoted at 90% confidence level unless otherwise stated.

## 2. Sample Properties and Data Reduction

The *Swift* satellite (Gehrels et al. 2004) is equipped with the wide-field ($120 \times 90$ deg$^2$) Burst Alert Telescope (BAT; Barthelmy et al. 2005). This telescope performs imaging in the 15–150 keV energy range and has been continuously observing the whole sky since its launch. The most recent catalog of sources detected in the BAT survey data is the 100 month catalog, which contains sources detected down to a flux limit $f \sim 3.3 \times 10^{-12}$ erg s$^{-1}$ cm$^{-2}$ in the 15–150 keV band.[4] With its combination of good sensitivity and all-sky coverage, this instrument provides an excellent view of the hard X-ray low-luminosity population in the nearby universe. We note that the 100 month BAT catalog is yet to be published (A. Segreto et al. 2017, in preparation), but all the data used in this work have been fully reprocessed.

We used the BAT_IMAGER code to reprocess the BAT survey 100 month data available in the HEASARC public archive (Segreto et al. 2010). This software has been developed to analyze data from coded mask instruments and performs screening, mosaicking, and source detection. The spectra used in this work are background subtracted and have been obtained by averaging over the whole BAT exposure. We used the official BAT spectral redistribution matrix.[5]

In Table 1 we report the list of sources we analyze in this work. From the *Swift*-BAT 100 month catalog we selected seven nearby AGNs ($z < 0.03$), associated to Seyfert 2 galaxies, lacking a *ROSAT* counterpart in the 0.1–2.4 keV band. Two of seven sources (ESO 116-G018 and NGC 5972) have never been observed before at 0.3–10 keV energies, and none have been previously observed using *Chandra*. The nearest source has $z = 0.0122$ (i.e., $d \sim 52$ Mpc), while the farthest has $z = 0.0297$ ($d \sim 130$ Mpc). The 15–55 keV luminosity range spans from $L_{\mathrm{BAT}} \sim 2 \times 10^{42}$ erg s$^{-1}$ to $L_{\mathrm{BAT}} \sim 2 \times 10^{43}$ erg s$^{-1}$. We selected low-redshift sources because the vast majority (>85%) of *Swift*-BAT-detected CT-AGNs have so far been discovered at $z < 0.04$ (see, e.g., Burlon et al. 2011; Ricci et al. 2015). Moreover, the lack of a *ROSAT* counterpart is a hint of at least moderate obscuration, with $N_{\mathrm{H}} \gtrsim 10^{22}$ cm$^{-2}$ (see, e.g., Figure 2 of Koss et al. 2016).

The sources were all targeted with 10 ks *Chandra* ACIS-S observations during *Chandra* Cycle 17 (Proposal number 17900432, P.I. Marco Ajello). The data were reduced with the CIAO (Fruscione et al. 2006) 4.7 software and the *Chandra* Calibration Data Base (`caldb`) 4.6.9, adopting standard procedures; no source showed significant pile-up, as measured by the CIAO PILEUP_MAP tool. Source and background spectra were extracted using the CIAO `specextract` tool. Source spectra were extracted in circular regions of 4″, while background was extracted from annuli with an internal radius $r_{\mathrm{int}} = 7''$ and external radius $r_{\mathrm{out}} = 20''$, after a visual inspection to avoid contamination from nearby sources. Point-source aperture correction was applied during the source spectral extraction process. Finally, the spectra were binned to have at least 15 bins in the *Chandra* spectrum: each bin contains 8 to 20 counts, according to the source brightness.

## 3. Spectral Fitting Results

In Table 2 we report the results of the spectral fitting of seven *Swift*-BAT Seyfert 2 galaxies in our sample. The spectral fitting was performed using XSPEC v. 12.9.0 (Arnaud 1996). Galactic absorption was determined using the Heasoft tool `nh` (Kalberla et al. 2005).

All sources were first fitted with a basic power law with photon index $\Gamma$ and intrinsic absorption $N_{\mathrm{H,z}}$ caused by the dusty torus surrounding the AGN accretion disk. The intrinsic

[4] http://bat.ifc.inaf.it/100m_bat_catalog/100m_bat_catalog_v0.0.htm

[5] http://heasarc.gsfc.nasa.gov/docs/heasarc/caldb/data/swift/bat/index.html

**Table 2**
Best-Fit Properties for the Seven Seyfert 2 Galaxies in Our Sample

| *Swift*-BAT ID | $N_{\rm H,gal}$ ($10^{20}$ cm$^{-2}$) | $N_{\rm H,z,\theta=90}$ ($10^{22}$ cm$^{-2}$) | $N_{\rm H,z,\theta=65}$ ($10^{22}$ cm$^{-2}$) | $\theta_{\rm max}$ (°) | $\Gamma$ | EW (keV) | $kT_{\rm BB}$ (keV) | SC | $\chi^2$/DOF | Model |
|---|---|---|---|---|---|---|---|---|---|---|
| NGC 4785 | 12.2 | $41.38^{+10.94}_{-8.75}$ | $77.37^{+20.65}_{-16.47}$ | ⋯ | $1.86^{+0.21}_{-0.19}$ | $0.48^{+0.33}_{-0.34}$ | ⋯ | $0.47 \pm 0.13$ | 7.9/15 | `po+MyT*(po+zga)` |
| ESO 500-G034 | 5.1 | $57.41^{+13.48}_{-10.80}$ | $107.60^{+25.26}_{-20.24}$ | 66 | $2.30^{+0.27}_{-0.24}$ | ⋯ | ⋯ | $0.18 \pm 0.06$ | 12.3/15 | `po+MyT*po` |
| NGC 1358 | 3.8 | $104.87^{+42.14}_{-35.80}$ | $196.44^{+211.09}_{-67.03}$ | 90 | $1.59^{+0.46}_{-0.45}$ | $0.75^{+0.75}_{-0.74}$ | $0.16^{+0.12}_{-0.11}$ | $0.77 \pm 0.42$ | 14.8/13 | `po+MyT*(bb+po+zga)` |
| ESO 116-G018 | 3.1 | $94.68^{+46.06}_{-39.97}$ | $178.13^{+86.19}_{-75.34}$ | 81 | $1.86^{+0.51}_{-0.48}$ | $1.41^{+2.67}_{-0.94}$ | ⋯ | $0.52 \pm 0.29$ | 17.2/14 | `po+MyT*(po+zga)` |
| ESO 119-G008 | 1.3 | $18.15^{+6.18}_{-5.49}$ | $34.02^{11.57}_{-10.28}$ | ⋯ | $1.77^{+0.21}_{-0.18}$ | ⋯ | ⋯ | $0.39 \pm 0.10$ | 17.7/20 | `po+MyT*po` |
| ESO 533-G050 | 1.5 | $22.56^{+5.45}_{-4.74}$ | $42.24^{+10.23}_{-8.88}$ | ⋯ | $1.65^{+0.18}_{-0.14}$ | $0.15^{+0.17}_{-0.15}$ | ⋯ | $0.54 \pm 0.12$ | 25.6/22 | `MyT*(po+zga)` |
| NGC 5972 | 3.0 | $78.62^{+16.94}_{-12.34}$ | $147.27^{+79.89}_{-59.22}$ | 72 | $1.63^{+0.23}_{-0.09}$ | ⋯ | $0.14^{+0.07}_{-0.05}$ | $0.65 \pm 0.35$ | 17.6/16 | `po+MyT*(bb+pexr)` |

**Note.** The XSPEC components reported in the "Model" columns are: `pow` is a power law with photon index $\Gamma$; when two power laws are present, their photon index is the same. `zga` is the `MyTorus` Iron $K\alpha$ component with equivalent width EW. `bb` is a black body component with a temperature $kT_{\rm BB}$ and fitting a soft excess observed below 1 keV. `pexr` is a power law with a cold matter reflection component. The intrinsic absorption $N_{\rm H,z}$ is modeled with `MyTorus` (`MyT` in the table), with an inclination angle $\theta$ equal to 65° or to 90°. $\theta_{\rm max}$ is the maximum inclination angle for which $N_{\rm H,z} > 10^{24}$ cm$^{-2}$. SC is the spectral curvature value computed following Koss et al. (2016).

absorption was computed using the MyTorus model (Murphy & Yaqoob 2009), which assumes a toroidal distribution of the absorbing material and is particularly effective in fitting spectra of heavily obscured objects.

We determined that for all seven sources in the sample, more complex models than the basic absorbed power law were required to significantly improve the fit. The significance of the additional components was verified performing an F-test, when statistically possible; in the remaining cases (i.e., when a Gaussian or a reflection component was added; see Protassov et al. 2002) the fits without the additional components always had reduced $\chi^2$, $\chi^2$/(degrees of freedom) >1.5, while the best fit with the additional component was reduced $\chi^2 \sim 1$.

The following are the different components we used in the fit, in addition to the basic absorbed power law. The best-fit models for each source are reported in Table 2.

1. Six spectra require a second power-law component, where photon index $\Gamma_2 = \Gamma_1$, the photon index of the main power law, and not affected by the intrinsic absorption $N_{\rm H,z}$. This second power law accounts for a fraction of AGN emission unabsorbed by the torus and/or for a scattered component (i.e., light deflected rather than absorbed by the dust and gas). The normalization of this second component is always <1% than the normalization of the main power law.
2. Four fits are significantly improved by adding the MyTorus fluorescent emission line component to model an excess in the spectrum at energy $E \sim 6.4$ keV. The line in the model was fixed at 6.4 keV (rest-frame) and accounts for the presence of the iron K$\alpha$ line. The iron K$\alpha$ equivalent width varies in the range EW = [0.15–0.75] keV (we report the EW values in Table 2).
3. Two sources in the sample require the addition of a black body component with $kT < 0.3$ keV to model the characteristic "soft excess" commonly observed in the AGN spectra and possibly due to the presence of warm gas close to the AGN accretion disk or in the BLR (see, e.g., Risaliti & Elvis 2004, p. 187). To understand the origin of this excess for these two sources (NGC 1358 and NGC 5972), we used the equations reported in Lehmer et al. (2010) to quantify the expected contribution of star-forming (SF) processes to the X-ray emission. We used the IRAS 8–1000 $\mu$m luminosities to compute the star formation rate (SFR), and SFR to estimate $L^{\rm SF}_{2-10\,\rm keV}$. For both sources, we find $L^{\rm SF}_{2-10\,\rm keV} \leqslant 10^{39}$ erg s$^{-1}$ (i.e., $\lesssim$0.1% of the AGN luminosity in the energy range), therefore safely ruling out a significant SF contribution to the X-ray emission.
4. One source in the sample (NGC 5972) showed an excess in the *Swift*-BAT spectrum at $E \sim 30$ keV, which is best-fitted with the PEXRAV model (Magdziarz & Zdziarski 1995), which parametrizes a power law with a significant reflection component. This reflection component is caused by cold material surrounding the accretion disk. Due to the low statistics of the spectrum of NGC 5972, we fixed the reflection scaling factor $R$ to 1. Because $R = \Omega/2\pi$, where $\Omega$ is the solid angle of the cold material, which is responsible for the reflection visible from the hot corona, which is responsible from the X-ray emission, $R = 1$ is the case where the reflection is produced by an infinite slab isotropically illuminated by the corona emission.

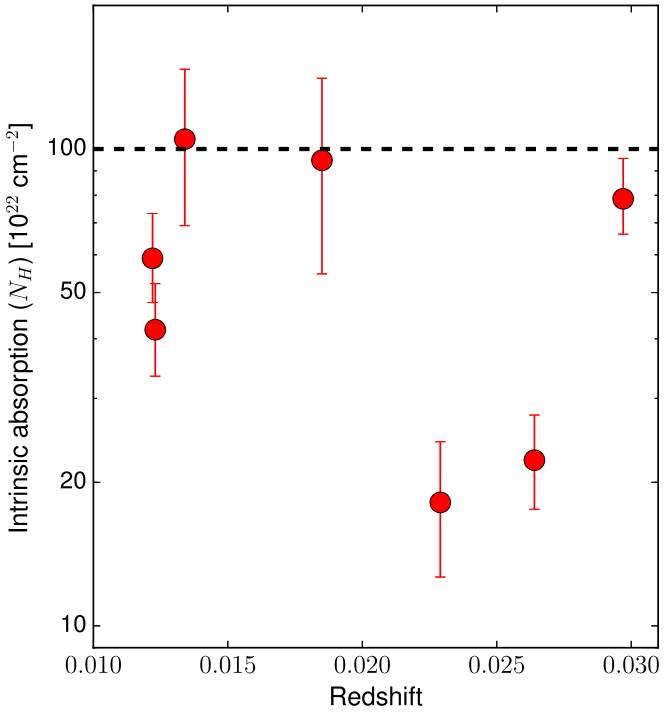


**Figure 1.** Intrinsic absorption $N_{\rm H,z}$ computed assuming $\theta = 90°$ as a function of redshift for the seven sources in our sample. The horizontal dashed line marks the Compton-thick regime (i.e., $N_{\rm H,z} \geqslant 10^{24}$ cm$^{-2}$).

Because the *Swift*-BAT spectrum is averaged on 100 months of observations, while the *Chandra* spectrum is obtained by a single observation, the joint fit of the *Chandra* and *Swift*-BAT spectra requires the addition of a multiplicative constant ($C_{\rm BAT}$) to the *Swift*-BAT spectrum to account for both flux variability and cross-correlation offsets. We examined the *Swift*-BAT light curves of the seven sources in our sample and none showed strong flares, with the flux variability limited to 20%–40%. For five of seven sources, the best-fit constant we obtained was consistent (within the errors) to $C_{\rm BAT} = 1$ and could be explained with the variability observed in the *Swift*-BAT light curves. For two AGNs (NGC 1358 and ESO 116-G018), however, the best-fit constant we found was significantly higher: ~9 and ~3, respectively. Such a high variability cannot be ruled out on the basis of our observations, because NGC 1358 and/or ESO 116-G018 could be changing-look AGNs (i.e., sources with a significant change in flux and/or amount of obscuring material); however, similar flux variations are extremely unlikely in highly obscured sources, because the reflection component washes out fluctuations on short timescales (see, e.g., Gandhi et al. 2015). Therefore, we fixed $C_{\rm BAT}$ to 1 for these two sources.

In Figure 1 we show the $N_{\rm H,z}$ distribution versus redshift for the sources in our sample, and report the seven spectra and their best fits in Figures 2 and 3. In the inset, we report the confidence contours for $\Gamma$ and $N_{\rm H,z}$; as can be seen, all the sources are heavily obscured. We discuss the $N_{\rm H,z}$ measurements in detail in the next section. Here we point out that, as a consequence of the heavy obscuration that affects mainly the 0.3–7 kev band, the ratio between the flux in the 15–150 keV band and the flux in the 0.3–7 keV one is >10 for all the

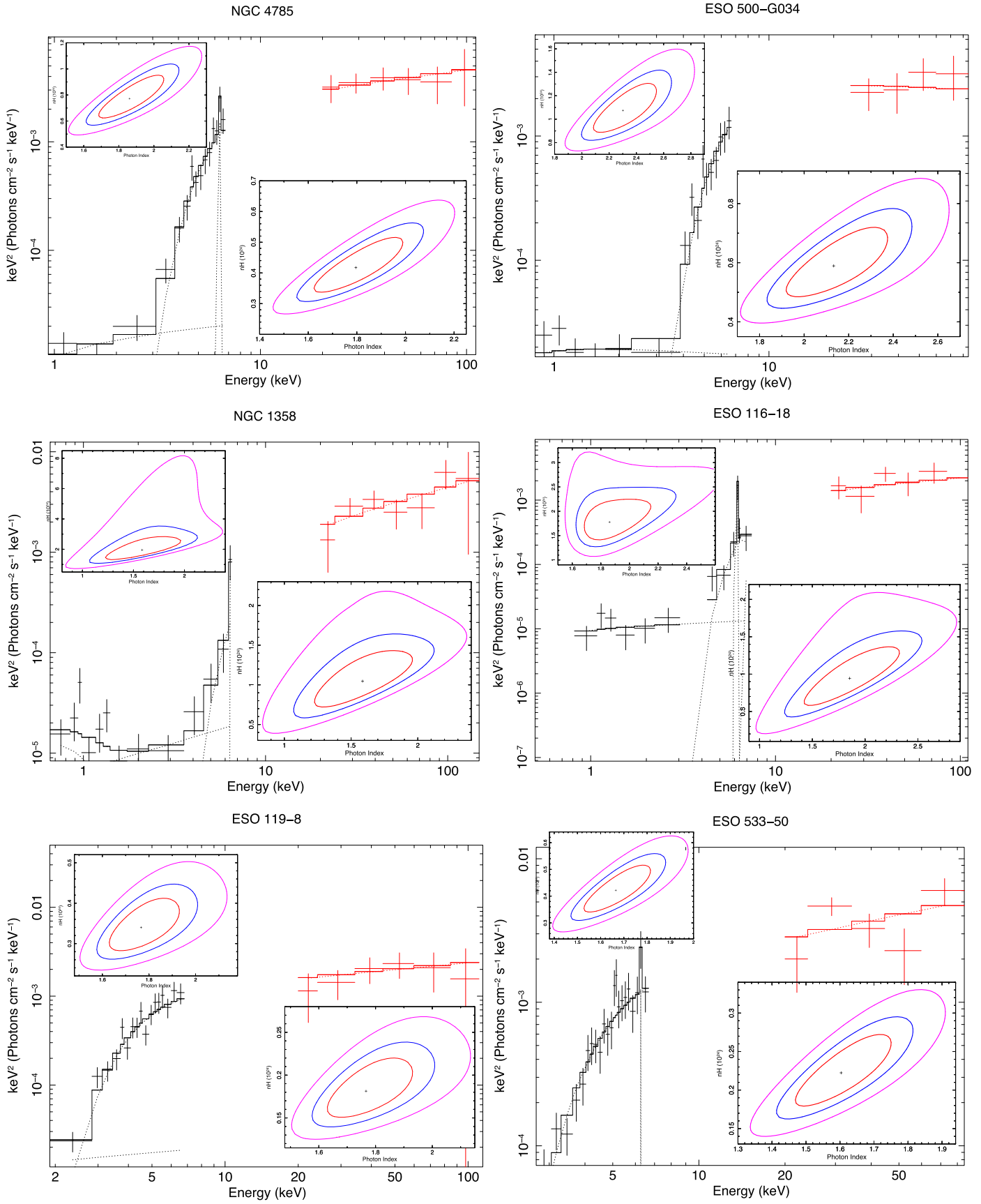


**Figure 2.** *Chandra* (black) and *Swift*-BAT (red) spectra for six of the seven sources in our sample. The best-fitting model is plotted as a solid line, while the single components are plotted as dotted lines. In the inset, the confidence contours at 68%, 90%, and 99% confidence level are shown for $\Gamma$ and $N_{\rm H,z}$ (in units of $10^{24}$ cm$^{-2}$), assuming $\theta = 90°$ (bottom right) and $\theta = 65°$ (top left).

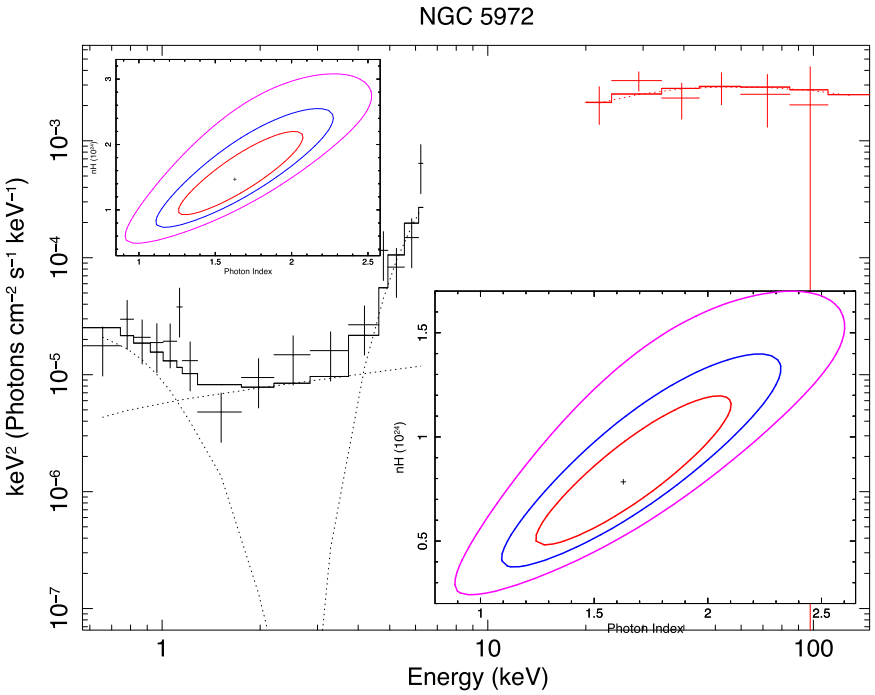


**Figure 3.** *Chandra* (black) and *Swift*-BAT (red) spectra of NGC 5972. The best-fit model is plotted as a solid line, while the single components are plotted as dotted lines. In the inset, the confidence contours at 68%, 90%, and 99% confidence level are shown for $\Gamma$ and $N_{\rm H,z}$ (in units of $10^{24}$ cm$^{-2}$), assuming $\theta = 90°$ (bottom right) and $\theta = 65°$ (top left).

sources in our sample and even >30 for the three most obscured objects.

### 3.1. Intrinsic Absorption and its Trend with Torus Inclination Angle

One of the MyTorus model parameters is $\theta$ (i.e., the inclination angle between the observer line of sight and the torus symmetry axis), where $\theta = 0°$ is a face-on observing angle and $\theta = 90°$ is an edge-on observing angle. The torus opening angle is $\theta = 60°$, while $\theta = 61°$ is the lowest angle for which the observer line of sight intercepts the torus.

The quality of our spectra does not allow us to constrain $N_{\rm H,z}$ and $\theta$ simultaneously. Therefore, we fit our data twice: first assuming $\theta = 90°$ (i.e., the edge-on scenario), and then second with $\theta = 65°$ (i.e., an angle closer to the angle for which the observer line of sight intercepts the torus). As can be seen in Table 2, assuming $\theta = 65°$ implies obtaining best-fit $N_{\rm H,z}$ values that are about two times higher than those obtained assuming $\theta = 90°$.

As already pointed out in the previous section, all sources in our sample are heavily obscured. Even in the worst-case scenario (i.e., assuming that all sources are observed edge-on; $\theta = 90°$), the objects all have $N_{\rm H,z} > 10^{23}$ cm$^{-2}$ at a 99% confidence level. Moreover, four of seven sources could be CT-AGNs, assuming that we are observing them with a $\theta$ close to the torus opening angle; in such a scenario, the path of the photons across the torus and the intrinsic absorption value would be, respectively, smaller and larger than in the case with $\theta = 90°$.

To complete our analysis, we refit the spectra with other two models to describe the absorbed power law: The first is the standard photoelectric absorption (zwabs in XSpec) and the other is pclabs, which describes the X-ray emission of an isotropic source of photons, corrected by the absorption caused by a spherical distribution of material. Compton scattering is taken into account in the second model. In both cases, we find that the $N_{\rm H,z}$ best-fit values are consistent (within the errors) with the MyTorus best-fit values obtained assuming $\theta = 90°$. These results may indicate that reliable $\theta$ values are closer to the $\theta = 90°$ limit than to the $\theta = 65°$ one. However, a proper disentanglement of the $N_{\rm H,z}$–$\theta$ can be broken only by increasing the 0.3–7 keV band exposure (see Section 4 for further details).

### 3.2. Comparison with Previous Results

Two sources in our sample have already been observed in the 0.5–10 keV band. In this section, we present previously published works and compare their results with our own.

NGC 1358 was targeted with a 10 ks XMM-*Newton* observation in 2005 (PI: I. Georgantopoulos), and the spectral fitting results for this observation (the *Swift*-BAT spectrum was not used in this work) were published in Marinucci et al. (2012). Their results are in good agreement with ours: They found that NGC 1358 was consistent with being a CT-AGNs, although with large uncertainties, with a best-fit intrinsic absorption of $N_{\rm H,z} = 1.3^{+8.5}_{-0.6} \times 10^{24}$ cm$^{-2}$.

NGC 4785 was studied by Gandhi et al. (2015), who combined the *Swift*-BAT observation used in this work with a 79 ks *Suzaku* observation. They fit the data with PEXRAV, using MyTorus and the TORUS model by Brightman & Nandra (2011). In all cases, they found that the source was CT, with the measured intrinsic absorption varying from $N_{\rm H,z} = 1.4^{+0.5}_{-0.9}$ cm$^{-2}$, while fitting the data with PEXRAV to $N_{\rm H,z} = 2.7^{+3.8}_{-0.8}$ cm$^{-2}$ and fitting the data with TORUS. Our $N_{\rm H,z}$ estimate is therefore consistent, within the errors, with their PEXRAV best fit, although it falls below their results with MyTorus and TORUS. While the

hypothesis that this discrepancy can be partially driven by the low statistics in our fit, which has only 16 degrees of freedom, compared with the 89 degrees in Gandhi et al. (2015), it is also possible that the change in the measured intrinsic absorption is due to intrinsic variability in the amount of obscuring material in the time between the *Suzaku* observation (2013 July) and the *Chandra* one (2016 April). A significant change in the AGN luminosity seems less likely, because the power-law photon index we measured ($\Gamma = 1.80^{+0.21}_{-0.19}$) is in good agreement with the one from Gandhi et al. (2015; $\Gamma = 2.1^{+0.4}_{-0.3}$ using `MyTorus`). Finally, Gandhi et al. (2015) found evidence of a strong Iron K$\alpha$ line in NGC 4785, with EW $= 1.1^{+u}_{-0.4}$ keV (where $u$ means unconstrained), while the EW of the line in our fit was weaker (EW $= 0.48^{+0.33}_{-0.34}$). This change in line intensity may strengthen the hypothesis that we are observing a variation in the amount of obscuring material, because CT-AGNs usually show prominent iron lines with EW $> 1$ keV (see, e.g., Koss et al. 2016).

## 4. Discussion and Conclusions

In this work, we presented the spectral fitting over the 0.3–150 keV energy range, which were obtained by combining *Chandra* and *Swift*-BAT observations, for seven AGNs at $z < 0.03$ selected from the 100 month *Swift*-BAT all-sky survey catalog. These sources were associated to Seyfert 2 galaxies and lacked a *ROSAT* counterpart in the 0.1–2.4 keV band. The combined *Chandra* and *Swift*-BAT spectra were then fit with different models to estimate spectral parameters, such as the spectral photon index $\Gamma$ and the intrinsic absorption $N_{\rm H,z}$.

As discussed in Section 3.1, all sources in the sample were heavily obscured; even in the (unlikely) scenario that all sources were edge-on (i.e., with inclination angle $\theta = 90°$) the less obscured object (ESO 119-G008) has $N_{\rm H,z} = 1.82^{+0.62}_{-0.55} \times 10^{23}\,{\rm cm}^{-2}$ and all sources have $N_{\rm H,z} > 10^{23}\,{\rm cm}^{-2}$ at a 99% confidence level. Moreover, one source (NGC 1358) had a best-fit intrinsic absorption $N_{\rm H,z} = 1.05^{+0.42}_{-0.36} \times 10^{24}\,{\rm cm}^{-2}$, which is consistent with being a CT-AGN.

We performed another fitting analysis by varying $\theta$ in 1° steps, and found that five of the sources in our sample could be CT-AGNs, if the inclination angle $\theta$ between the observer line of sight and the torus rotation axis was small enough (see column $\theta_{\rm max}$ in Table 2).

A first important result of this work is therefore finding an effective way to detect obscured AGNs in the nearby universe by taking advantage of the combination of low limiting flux and wide field of view in the *Swift*-BAT all-sky survey. It is worth noting that while our selection technique detects a population of sources with $N_{\rm H,z} > 10^{23}\,{\rm cm}^{-2}$, the observed fraction of unobscured AGNs (i.e., with $N_{\rm H,z} < 10^{22}\,{\rm cm}^{-2}$) obtained without applying any selection criteria was 35%–55% (Burlon et al. 2011).

Koss et al. (2016) developed a technique to identify CT-AGNs in AGNs with low count statistics observed by *Swift*-BAT or *NuSTAR*, and found that the fraction of CT-AGNs at $z < 0.03$ was ∼22%. The Koss et al. (2016) method is based on the curvature of the AGN spectrum between 14 and 50 keV, parametrized as follows:

$$SC_{\rm BAT} = \frac{-3.42A - 0.82B + 1.65C + 3.58D}{\rm Tot}, \qquad (1)$$

where $A$, $B$, $C$, $D$, and Tot are the count rates measured with *Swift*-BAT in the 14–20 keV, 20–24 keV, 24–35 keV, 35–50 keV, and 14–50 keV, respectively. $SC_{\rm BAT} = 0.4$ is the CT-AGN selection threshold. In Koss et al. (2016), seven of the nine sources with $SC_{\rm BAT} > 0.4$ have $N_{\rm H,z} > 10^{24}\,{\rm cm}^{-2}$, and the remaining two are significantly obscured ($N_{\rm H,z} > 5 \times 10^{23}\,{\rm cm}^{-2}$).

In Table 2 we report $SC_{\rm BAT}$ values for the seven sources in our sample, and the Koss et al. (2016) assumption on $SC_{\rm BAT}$ was supported by our results. In fact, the most obscured source in our sample (NGC 1358) has $SC_{\rm BAT} = 0.77 \pm 0.42$ (i.e., which was our highest $SC_{\rm BAT}$ value), although the uncertainty on the SC value is quite large. Two other highly obscured sources (ESO 116-G018 and NGC 5972) also have $SC_{\rm BAT} > 0.4$ ($SC_{\rm BAT} = 0.52 \pm 0.29$ and $SC_{\rm BAT} = 0.65 \pm 0.35$, respectively), although they have $SC_{\rm BAT} < 0.4$ at a 90% confidence level. These two objects have $N_{\rm H,z} < 10^{24}\,{\rm cm}^{-2}$ assuming $\theta = 90°$, but may have $N_{\rm H,z} > 10^{24}\,{\rm cm}^{-2}$ assuming reasonable values of $\theta$ (81° and 72°, respectively). Finally, two sources with $SC_{\rm BAT} > 0.4$, and therefore candidate CT-AGNs according to the Koss et al. (2016) equation, have $N_{\rm H,z} \sim 2$–$4 \times 10^{23}\,{\rm cm}^{-2}$ assuming $\theta = 90°$.

The results of this work represent the first step for identifying and analyzing CT-AGNs in the local universe. To improve our findings, we plan to extend our analysis in two ways:

1. Increasing the exposure for the objects we described in this work using XMM-*Newton*, *Chandra*, and *NuSTAR*. The 0.3–7 keV spectra we studied were obtained with observations of only 10 ks each, and have between 80 (for the two most obscured AGNs in our sample) and 270 (ESO 533-G050) net counts in the 0.3–7 keV band. Breaking the degeneracy between the intrinsic absorption $N_{\rm H,z}$ and the inclination angle $\theta$, and therefore assessing whether a source is a CT-AGNs, requires larger count statistics. In comparison, Tanimoto et al. (2016) simultaneously constrained $N_{\rm H,z}$ and $\theta$ for the three candidate CT-AGNs that were observed with *Suzaku* for 30–70 ks and each had about 500 net counts in the 0.3–7 keV band.
2. Increasing the sample of candidate CT-AGNs. The selection criteria we adopted in this work proved very effective, and the *Swift*-BAT 100 month catalog contains another ∼5–10 sources at $z < 0.04$ that are Seyfert 2 galaxies lacking a *ROSAT* counterpart and that have not been observed by either *Chandra* or XMM-*Newton*. We plan to target these sources with future *Chandra* and XMM-*Newton* observations.

## References


Aird, J., Alexander, D. M., Ballantyne, D. R., et al. 2015, ApJ, 815, 66
Ajello, M., Greiner, J., Sato, G., et al. 2008, ApJ, 689, 666
Alexander, D. M., Bauer, F. E., Brandt, W. N., et al. 2003, AJ, 126, 539
Annuar, A., Gandhi, P., Alexander, D. M., et al. 2015, ApJ, 815, 36
Arévalo, P., Bauer, F. E., Puccetti, S., et al. 2014, ApJ, 791, 81
Arnaud, K. A. 1996, in ASP Conf. Ser. 101, Astronomical Data Analysis Software and Systems V, ed. G. H. Jacoby & J. Barnes (San Francisco, CA: ASP), 17
Baloković, M., Comastri, A., Harrison, F. A., et al. 2014, ApJ, 794, 111
Barthelmy, S. D., Barbier, L. M., Cummings, J. R., et al. 2005, SSRv, 120, 143
Bauer, F. E., Arévalo, P., Walton, D. J., et al. 2015, ApJ, 812, 116
Blandford, R. D., & Begelman, M. C. 1999, MNRAS, 303, L1
Boorman, P. G., Gandhi, P., Alexander, D., et al. 2016, ApJ, 833, 245
Brightman, M., Baloković, M., Stern, D., et al. 2015, ApJ, 805, 41
Brightman, M., & Nandra, K. 2011, MNRAS, 413, 1206
Buchner, J., Georgakakis, A., Nandra, K., et al. 2015, ApJ, 802, 89
Burlon, D., Ajello, M., Greiner, J., et al. 2011, ApJ, 728, 58

Civano, F., Hickox, R. C., Puccetti, S., et al. 2015, ApJ, 808, 185
Comastri, A. 2004, in Supermassive Black Holes in the Distant Universe, ed. A. J. Barger (Dordrecht: Kluwer), 245
Della Ceca, R., Caccianiga, A., Severgnini, P., et al. 2008, A&A, 487, 119
Elitzur, M., & Ho, L. C. 2009, ApJL, 701, L91
Elitzur, M., & Shlosman, I. 2006, ApJL, 648, L101
Emmering, R. T., Blandford, R. D., & Shlosman, I. 1992, ApJ, 385, 460
Fruscione, A., McDowell, J. C., Allen, G. E., et al. 2006, Proc. SPIE, 6270, 62701V
Gandhi, P., Lansbury, G. B., Alexander, D. M., et al. 2014, ApJ, 792, 117
Gandhi, P., Yamada, S., Ricci, C., et al. 2015, MNRAS, 449, 1845
Gehrels, N., Chincarini, G., Giommi, P., et al. 2004, ApJ, 611, 1005
Georgantopoulos, I., Comastri, A., Vignali, C., et al. 2013, A&A, 555, A43
Gilli, R., Comastri, A., & Hasinger, G. 2007, A&A, 463, 79
Harrison, F. A., Aird, J., Civano, F., et al. 2016, ApJ, 831, 285
Hönig, S. F., & Beckert, T. 2007, MNRAS, 380, 1172
Kalberla, P. M. W., Burton, W. B., Hartmann, D., et al. 2005, A&A, 440, 775
Koss, M. J., Assef, R., Baloković, M., et al. 2016, ApJ, 825, 85
Koss, M. J., Romero-Cañizales, C., Baronchelli, L., et al. 2015, ApJ, 807, 149
Lansbury, G. B., Gandhi, P., Alexander, D. M., et al. 2015, ApJ, 809, 115
Lanzuisi, G., Ranalli, P., Georgantopoulos, I., et al. 2015, A&A, 573, A137
Lehmer, B. D., Alexander, D. M., Bauer, F. E., et al. 2010, ApJ, 724, 559
Magdziarz, P., & Zdziarski, A. A. 1995, MNRAS, 273, 837
Marinucci, A., Bianchi, S., Nicastro, F., Matt, G., & Goulding, A. D. 2012, ApJ, 748, 130
Matt, G., Pompilio, F., & La Franca, F. 1999, NewA, 4, 191
Mullaney, J. R., Del-Moro, A., Aird, J., et al. 2015, ApJ, 808, 184
Murphy, K. D., & Yaqoob, T. 2009, MNRAS, 397, 1549
Narayan, R., & Yi, I. 1994, ApJL, 428, L13
Nenkova, M., Sirocky, M. M., Ivezić, Ž., & Elitzur, M. 2008, ApJ, 685, 147
Nicastro, F. 2000, ApJL, 530, L65
Protassov, R., van Dyk, D. A., Connors, A., Kashyap, V. L., & Siemiginowska, A. 2002, ApJ, 571, 545
Puccetti, S., Comastri, A., Bauer, F. E., et al. 2016, A&A, 585, A157
Ricci, C., Bauer, F. E., Treister, E., et al. 2016, ApJ, 819, 4
Ricci, C., Ueda, Y., Koss, M. J., et al. 2015, ApJL, 815, L13
Risaliti, G., & Elvis, M. 2004, in Supermassive Black Holes in the Distant Universe, ed. A. J. Barger (Dordrecht: Kluwer), 187
Risaliti, G., Elvis, M., Fabbiano, G., et al. 2007, ApJL, 659, L111
Risaliti, G., Maiolino, R., & Salvati, M. 1999, ApJ, 522, 157
Segreto, A., Cusumano, G., Ferrigno, C., et al. 2010, A&A, 510, A47
Shakura, N. I., & Sunyaev, R. A. 1973, A&A, 24, 337
Tanimoto, A., Ueda, Y., Kawamuro, T., & Ricci, C. 2016, PASJ, 68, S26
Treister, E., Urry, C. M., & Virani, S. 2009, ApJ, 696, 110
Vasudevan, R. V., Brandt, W. N., Mushotzky, R. F., et al. 2013, ApJ, 763, 111
Vignali, C., Mignoli, M., Gilli, R., et al. 2014, A&A, 571, A34
Yaqoob, T., Murphy, K. D., Miller, L., & Turner, T. J. 2010, MNRAS, 401, 411